

Dipole-improved gating of azulene-based  
single-molecule transistors†Cite this: *J. Mater. Chem. C*, 2022,  
10, 7803Received 10th April 2022,  
Accepted 6th May 2022

DOI: 10.1039/d2tc01474b

rsc.li/materials-c

Huanyan Fu,<sup>‡ab</sup> Cong Zhao,<sup>‡a</sup> Jie Cheng,<sup>‡c</sup> Shuyao Zhou,<sup>‡b</sup> Peizhen Peng,<sup>c</sup>  
Jie Hao,<sup>a</sup> Zhirong Liu,<sup>id b</sup> Xike Gao,<sup>id \*c</sup> Chuancheng Jia<sup>id \*ab</sup> and  
Xuefeng Guo<sup>id \*ab</sup>

Single-molecule field-effect transistors (FETs) are promising to break the development bottleneck of device miniaturization, which is of great significance for realizing the development of more than Moore. However, the field-effect properties under gating need to be further improved. Here, we design an azulene-based single-molecule FET with two opposite dipole moments in a single molecule and ionic liquid gating. This kind of FET shows ambipolar characteristics and better gate controllability with a high on–off current ratio, which is about five times higher than that of single-molecule FET based on the naphthalene molecule. According to both experimental and theoretical research, the high efficiency of gate control is related to the inherent dipole moment of azulene, which results in a lower conductance in the off-state, higher polarizability of azulene, and an effective energy level shift of the molecule. These studies offer a proven method to build single-molecule FETs with high gating regulation efficiency, thus promoting the development of practical single-molecule electronic devices.

## Introduction

The original intention of molecular electronics is to use single molecules to construct electronic devices and realize the miniaturization of electronic devices.<sup>1–4</sup> Single-molecule field-effect transistors (FETs) have the potential to be used as core

elements for constructing logic circuits.<sup>5–7</sup> Due to the inherently small size of the single-molecule FET, it has the potential to extend Moore's law to the single-molecule level, breaking the development bottleneck of device miniaturization.<sup>8–12</sup> Meanwhile, it is also a powerful tool for exploring quantum transport and novel physical phenomena.<sup>13–19</sup> Therefore, single-molecule FETs have been widely studied. Single-molecule FETs are generally constructed by sandwiching a molecule between two electrodes, and the charge transport through the single molecule is regulated by the gate electric field. The working principle of the traditional silicon-based FETs is to control the carriers through the gate voltage, while the working principle of the single-molecule FETs is to control the relative position between the molecular energy level and the Fermi level of the electrode through the gate voltage in the tunnelling region.<sup>20–22</sup> In this working mechanism, the key development issue currently facing is how to improve the regulation efficiency of gating.

In order to efficiently realize the field-effect properties of single-molecule devices, the regulation efficiency of gating can be enhanced from two aspects. On the one hand, the gate in a single-molecule FET requires a better design to effectively apply a strong gate electric field to the single molecule. A lot of work has been done to overcome this challenge.<sup>6,12,23–25</sup> A typical example is the ionic liquid gate,<sup>26,27</sup> which modulates charge transport of the single-molecule FETs by utilizing the electrical double layer of ionic dielectrics. Since the thickness of the electrical double layer is at the molecular level and the capacitance is large, the electric field applied to the molecule can be quite strong.<sup>28</sup> On the other hand, the molecule in the single-molecule FETs should be redesigned to enhance the molecular response to the electric field,<sup>29,30</sup> such as increasing the polarizability of molecular orbitals.<sup>21,31</sup> In addition, to improve the on–off current ratio, which is a key parameter of the single-molecule FET, reducing the off-state current is an effective method. For instance, single-molecule FETs based on molecules with destructive quantum interference effects are designed and can exhibit low conductance in the off-state, leading to a high on–off current ratio.<sup>27</sup> To further improve the on–off current ratio of

<sup>a</sup> Center of Single-Molecule Sciences, Institute of Modern Optics, Frontiers Science Center for New Organic Matter, College of Electronic Information and Optical Engineering, Nankai University, 38 Tongyan Road, Jinnan District, Tianjin 300350, P. R. China. E-mail: guoxf@pku.edu.cn, jiacc@nankai.edu.cn

<sup>b</sup> Beijing National Laboratory for Molecular Sciences, National Biomedical Imaging Center, College of Chemistry and Molecular Engineering, Peking University, 292 Chengfu Road, Haidian District, Beijing 100871, P. R. China

<sup>c</sup> Key Laboratory of Synthetic and Self-Assembly Chemistry for Organic Functional Molecules, Shanghai Institute of Organic Chemistry, University of Chinese Academy of Sciences, Chinese Academy of Sciences, Shanghai 200032, China. E-mail: gaouxk@mail.sioc.ac.cn

† Electronic supplementary information (ESI) available. See DOI: <https://doi.org/10.1039/d2tc01474b>

‡ These authors contributed equally to this paper.

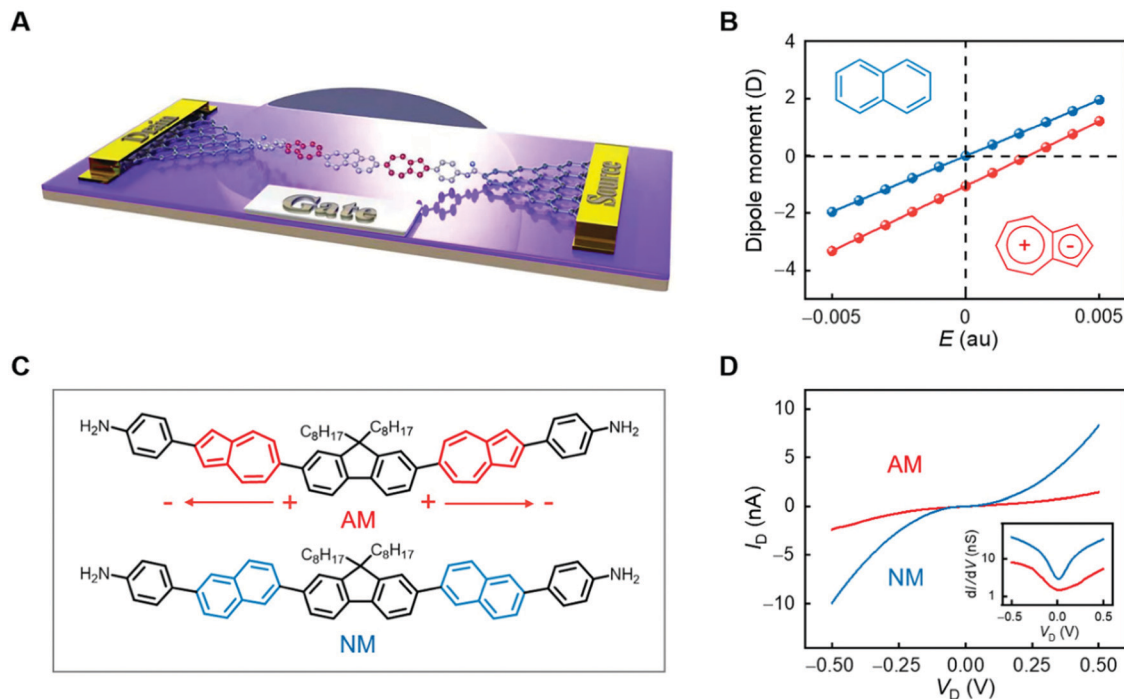


**Fig. 1** Structure and charge transport of single-molecule junctions. (A) Schematic illustration of the graphene-based single-molecule junction with ionic liquid gating. (B) Theoretical dipole moment versus electric field for azulene and naphthalene. (C) Molecular structures of AM and NM with amine terminal groups at both ends. (D) Experimental  $I$ - $V$  characteristics for AM-based single-molecule junction and NM-based single-molecule junction measured at 220 K at  $V_G = 0$  V. The inset shows corresponding differential conductance ( $dI/dV$ ) versus  $V_D$ .

single-molecule FETs, other possible factors that can enhance the gate controllability and reduce the off-state conductance need to be explored.

Azulene is an aromatic  $10\pi$ -electron system composed of a 5-membered ring and a 7-membered ring. The 5-membered ring possesses a partially localized negative charge, while the 7-membered ring possesses a partially localized positive charge, resulting in an inherent dipole moment of  $\sim 1.08$  D.<sup>32–35</sup> Furthermore, azulene has higher polarizability compared to the traditional aromatic naphthalene, an isomer of azulene that has no intrinsic dipole moment. From the theoretical calculation in Fig. 1B, it can be observed that the slope of azulene is larger than that of naphthalene, which represents the molecular response to the electric field. This shows that under different electric fields, the dipole moment of azulene changes greatly, indicating that the polarizability of azulene is higher. Here, we design single-molecule FETs based on azulene molecule (AM) and naphthalene molecule (NM), the latter being the control (Fig. 1C), with ionic liquid gating on the platform of graphene-based single-molecule junctions (SMJs) (Fig. 1A). The single-molecule transistors with ionic liquid that provides a strong gating electric field can achieve efficient regulation of charge transport. By designing two azulene groups in AM, two opposite dipole moments are located in the molecular charge transport channel to reduce the off-state conductance. According to the experimental and theoretical studies of the two systems, AM-based single-molecule FETs exhibit a higher on-off current ratio and better gate controllability compared with NM-based

single-molecule FETs, which is due to the reduced off-state conductance and more efficient energy level shift of AM with gating.

## Results and discussion

### 1. Design and construction of single-molecule FETs

The synthetic procedure of AM and NM is detailed in the ESI.† Stable single-molecule junctions were constructed by connecting AM or NM to graphene electrodes through covalent amide bonds (detailed fabrication process in Fig. S2 and S3, ESI†). A small droplet of ionic liquid is placed on the array of graphene-based devices and the gate electrode (Fig. S4, ESI†). *N,N*-Diethyl-*N*-(2-methoxyethyl)-*N*-methylammonium bis-(trifluoromethylsulfonyl)-imide (DEME-TFSI) (detailed structure in Fig. S5, ESI†) is chosen as ionic liquid because the similar sizes of positive and negative ions ( $\sim 7.5$  Å) can maintain a symmetric electrical double layer (EDL) under opposite gate voltages. More importantly, the thickness of the geometric EDL is  $\sim 7.5$  Å, which is much less than the molecular length ( $\sim 30$  Å), thus providing a strong electric field to modulate charge transport through single molecules. From the experimental  $I$ - $V$  characteristics, both molecules are proved to be connected to the graphene electrodes (Fig. 1D), and the AM-based single-molecule junction exhibits a lower current than the NM-based junction. Correspondingly, the differential conductance for AM is much lower than that for NM (Fig. 1D inset). On the one hand, it is because the symmetrical

dipole moments of AM can suppress the current. On the other hand, the dominant transport orbital p-HOMO of AM is farther away from the Fermi level (Fig. 4B) and more localized (Fig. S7A and C, ESI†) than NM. Therefore, by symmetrically designing two azulenes with intrinsic opposite dipole moments in AM (Fig. 1B and C), the conductance of the device is successfully reduced, providing a basis for good field-effect properties.

## 2. Field-effect characteristics of single-molecule FETs

Transfer characteristic is an important parameter to evaluate the performance of field-effect transistors. It refers to the modulation of current by the gate voltage ( $V_G$ ) when the bias voltage ( $V_D$ ) is fixed. The transfer characteristics of the AM-based single-molecule FET at different bias voltages are shown in Fig. 2B. It can be observed that as the  $V_G$  increases from  $-2$  V to  $2$  V, the current decreases and then increases, forming the lowest current point near  $V_D = 1$  V. Similar behavior occurs in the NM-based single-molecule FET (Fig. 3B), but the lowest current point for NM is always higher than that for AM, regardless of the bias voltage. Additionally, the current variation of NM is less sensitive to the gate voltage than that of AM, which might be related to the higher polarizability of AM. Furthermore, the on-off current ratio, that is, the ratio of maximum and minimum value of  $|I_D|$ , varies with the applied bias voltage and has a maximum value near the zero-bias voltage point. The highest on-off current ratio for NM is  $\sim 36$  (Fig. 3B inset), while the highest on-off ratio for AM reaches  $\sim 200$  (Fig. 2B inset), which is 5.5 times of the NM value.

The change of the on-off current ratio with bias voltages indicates that the gate controllability of both single-molecule FETs decreases with the increasing bias voltage. In another word, as the bias voltage increases, the conductance of the single molecular junction is less sensitive to the gate voltage. This huge difference in on-off current ratios should be related to unique symmetric dipole moments, as AM with symmetric dipole moments has a lower current in the off-state in comparison with NM without dipole moments, resulting in a higher on-off current ratio. In addition, the control system with a non-symmetric structure shows that the on-off current ratio is related to the orientation of dipole moments (Fig. S8 and S9, ESI†). This result is consistent with the previous prediction, proving that the current in the off-state can be lowered and the on-off current ratio of the single-molecule FET can be significantly improved by introducing two opposite dipole moments in the molecular junction.

The field-effect properties of the single-molecule transistors are further studied to reveal more charge transport properties and understand the mechanisms. The changes in  $I_D$ - $V_D$  characteristics and the changes in differential conductance  $dI/dV$  versus  $V_D$  with the gate voltages for AM-based single-molecule FETs are shown in Fig. 2C and D, respectively. As can be observed in these figures, the conductance decreases and then increases as the gate voltage  $V_G$  changes from  $-2$  V to  $2$  V for the AM-based single-molecule FET. The turning point is  $0$  V. Similarly, when  $V_G$  changes from  $-2$  V to  $2$  V, the conductance of NM decreases and then increases after  $V_G = 1$  V (Fig. 3C and D).

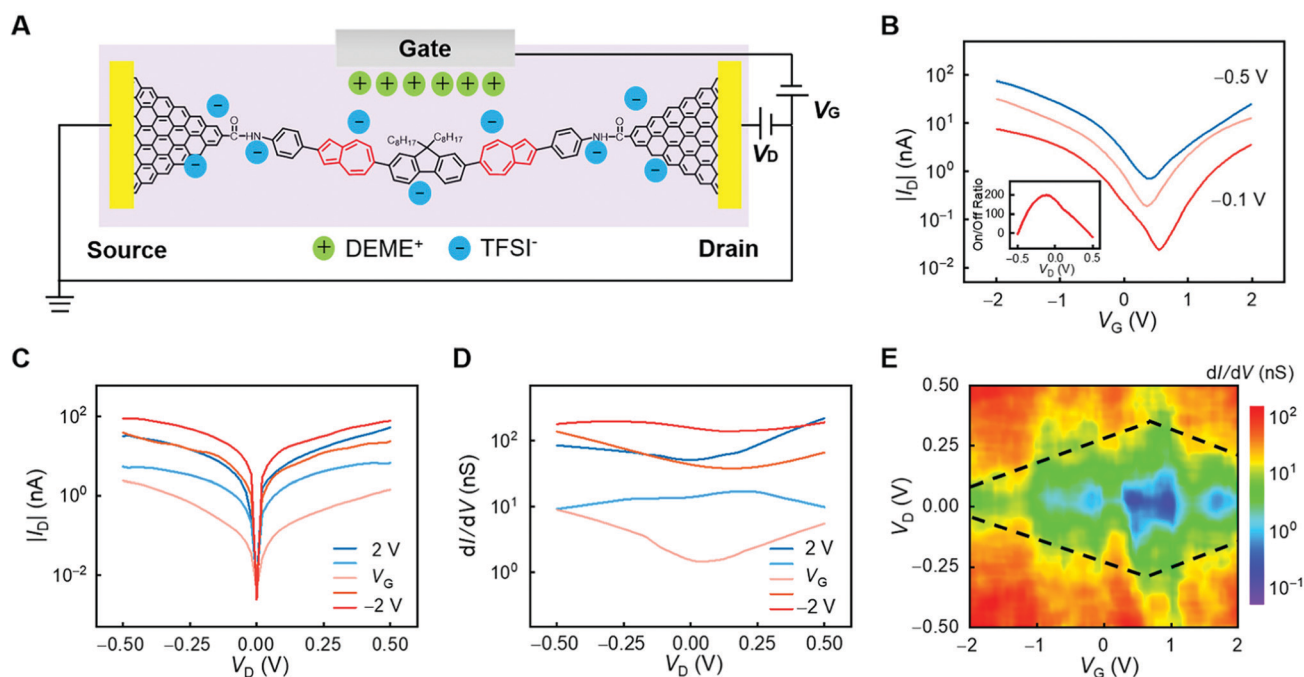


**Fig. 2** Field-effect characteristics of AM-based single-molecule FETs. (A) Schematic illustration of the AM-based single-molecule FET with ionic liquid gating. (B) Transfer characteristics at  $V_D = -0.1, -0.3$  and  $-0.5$  V. Inset shows  $V_D$ -dependent on-off current ratio. (C)  $|I_D|$  versus  $V_D$  characteristics at  $-2 \text{ V} \leq V_G \leq 2 \text{ V}$  with a step of  $1 \text{ V}$ . (D) Corresponding differential conductance ( $dI/dV$ ) characteristics at  $-2 \text{ V} \leq V_G \leq 2 \text{ V}$  with a step of  $1 \text{ V}$ . (E) Two-dimensional visualization of  $dI/dV$  plotted versus  $V_G$  and  $V_D$ . The dashed lines represent the boundary between resonant transmission and non-resonant transmission.

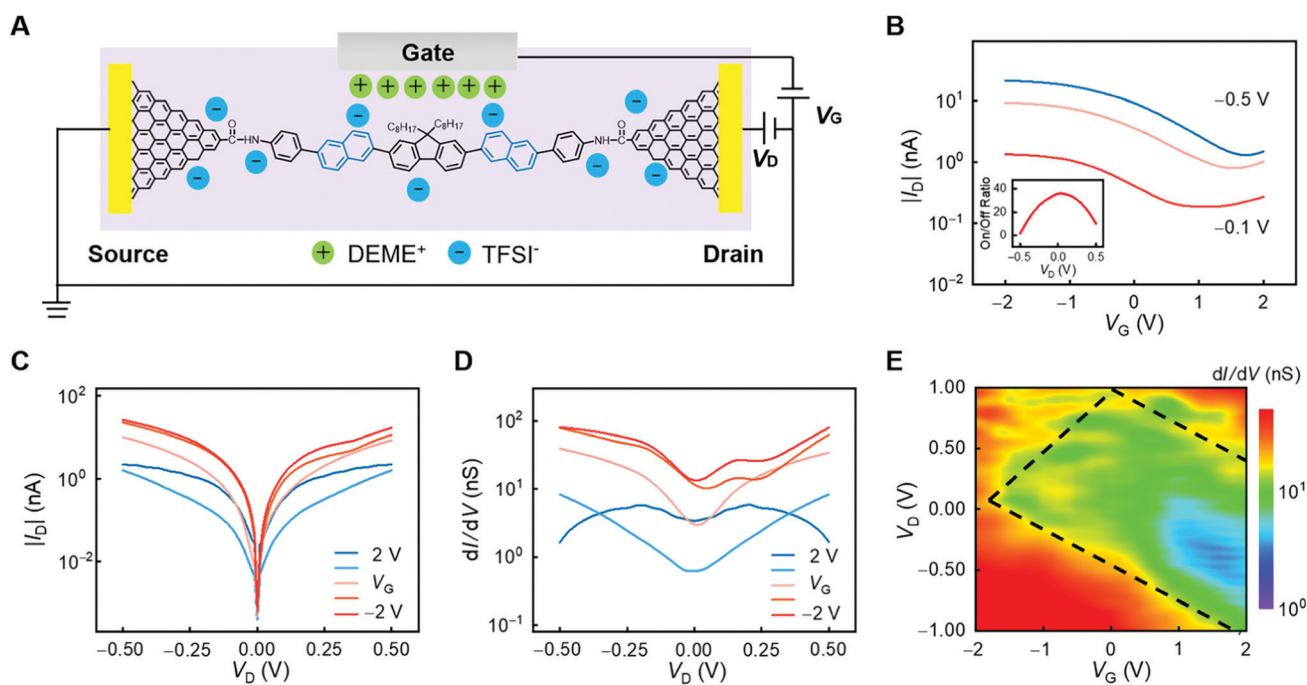


**Fig. 3** Field-effect characteristics of NM-based single-molecule FETs. (A) Schematic illustration of the NM-based single-molecule FET with ionic liquid gating. (B) Transfer characteristic at  $V_D = -0.1, -0.3$  and  $-0.5$  V. Inset shows  $V_D$ -dependent on-off current ratio. (C)  $|I_D|$  versus  $V_D$  characteristics at  $-2 \text{ V} \leq V_G \leq 2 \text{ V}$  with a step of 1 V. (D) Corresponding differential conductance ( $dI/dV$ ) characteristics at  $-2 \text{ V} \leq V_G \leq 2 \text{ V}$  with a step of 1 V. (E) Two-dimensional visualization of  $dI/dV$  plotted versus  $V_G$  and  $V_D$ . The dashed lines represent the boundary between resonant transmission and non-resonant transmission.

Different turning points indicate that the abilities of gate control and the molecular orbital characteristics for AM and NM may be different. The two-dimensional conductance mapping of differential conductance  $dI/dV$  versus  $V_G$  and  $V_D$  for both AM and NM are further plotted to show the results more visualized (Fig. 2E and 3E). The low-conductance regions in blue and green show off-resonant transport through the highest occupied molecular orbital (HOMO) or the lowest unoccupied molecular orbital (LUMO), while the high-conductance regions in orange and red indicate that the conductive frontier molecular orbital of the molecule shifts to the bias window. For AM, the low-conductance region shows a nearly complete diamond shape in the 2D conductance mapping, indicating either HOMO or LUMO contributing to the charge transport can enter the bias window at certain gate voltages. For NM, the diamond shape is not complete, which means only HOMO can be modulated into the bias window by the gate. Therefore, only AM-based FET exhibits ambipolar characteristics and can be tuned more efficiently by the gate, which is in agreement with the prediction that the polarizability of the molecule can enhance the molecular response to the electric field, thus improving the gate control.

### 3. Working mechanism of single-molecule FETs

The different field-effect behaviors of AM and NM can not only be explained by the different dipole moment and polarizability that are discussed in the previous section, but are also related to the shift of energy levels. To further understand the difference, the field-effect properties of two single-molecule FETs are

theoretically simulated. As is illustrated in Fig. 4A, the molecular energy levels can be regulated by the gate voltages. When the molecular energy level, either HOMO or LUMO, shifts into or just approaches the bias window, the conductance will be enhanced. Specifically, when  $V_G$  is negative, the molecular energy levels shift upwards. In this case, HOMO is close to the bias window and becomes the dominant charge transport channel, while LUMO is far away from the bias window. When  $V_G$  is positive, they move in the opposite direction and LUMO is closer. Thus, the relationship between molecular levels and the Fermi level of graphene is of great significance. By calculating the energy bandgaps of these two molecules and comparing them with the Fermi level of graphene (Fig. 4B), it is obvious that the Fermi level of graphene is between the HOMO and LUMO of the two molecules. Theoretically, by applying different gate voltages, the molecular orbitals can be tuned close to the Fermi level of graphene. As is shown in Fig. 4B, the bandgap of NM reaches  $\sim 3.64$  eV, while the bandgap of AM is only  $\sim 2.98$  eV. The HOMOs of both molecules are close to the Fermi level of graphene, thus the LUMO of AM is much closer to the Fermi level of graphene than that of NM. Therefore, modulating the LUMO of AM to the Fermi level of graphene requires a lower gate voltage, which is the reason why the AM-based single-molecule FET exhibits ambipolar properties.

Since zero-bias transmission spectra can show the energy level shift and charge transport mechanism more clearly, the transmission spectra at different gate voltages for AM and NM were simulated (Fig. 4C and D). The p-LUMO and p-HOMO of

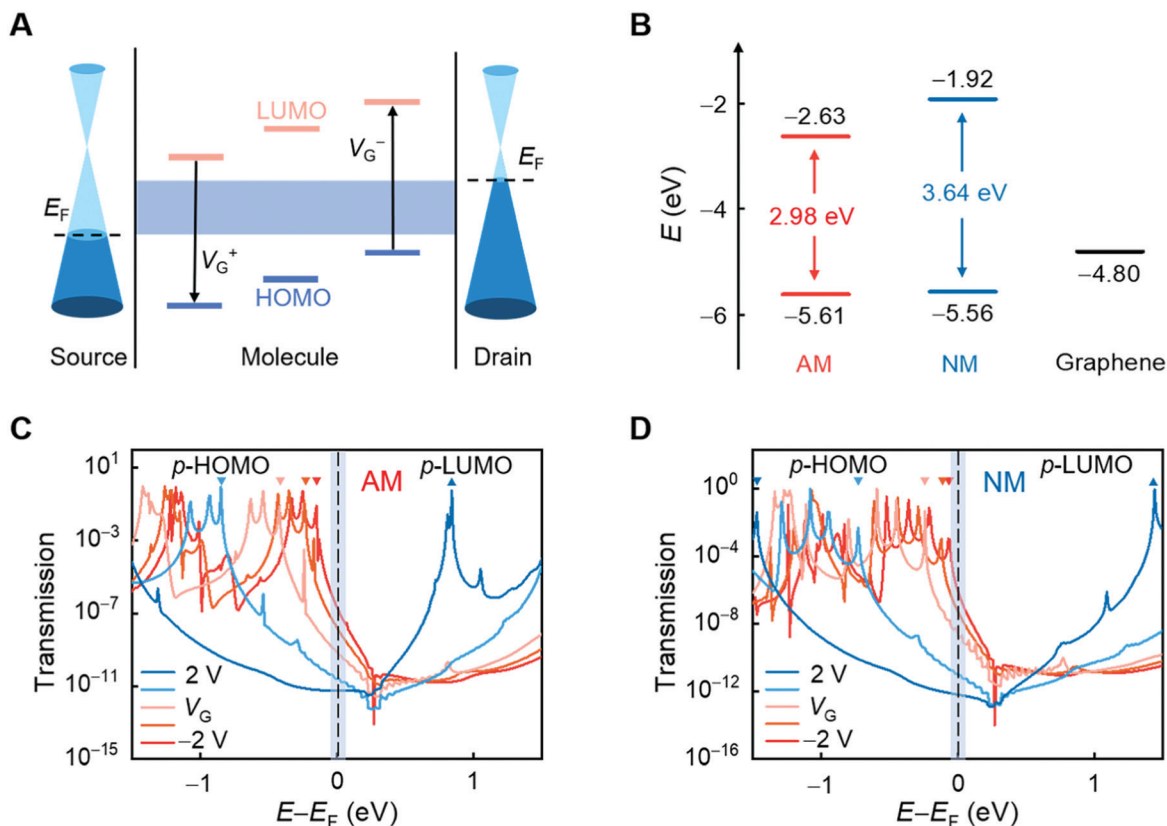


Fig. 4 Working mechanism for single-molecule FETs. (A) Schematic band diagram of molecular orbitals relative to the Fermi level of graphene electrode under different gating. (B) Calculated molecular orbital energy levels of isolated molecules, and the Fermi level of graphene deduced from experiment results. (C) Gate-dependent zero-bias transmission spectroscopies for AM-based single-molecule junctions at  $-2 \text{ V} \leq V_G \leq 2 \text{ V}$  with a step of  $1 \text{ V}$ . (D) Gate-dependent zero-bias transmission spectroscopies for NM-based single-molecule junctions at  $-2 \text{ V} \leq V_G \leq 2 \text{ V}$  with a step of  $1 \text{ V}$ . The downward triangles mark p-HOMO and upward triangles mark p-LUMO.

AM are higher than those of NM. In particular, the p-HOMO is the dominant transport molecular orbital that determines the on-state current. Therefore, the on-state current of AM is higher than that of NM. Furthermore, for AM-based single-molecule FETs, the off-state current is lower than that of NM because the symmetric dipole moments of AM can suppress the current. All of these reasons result in a higher on-off current ratio for AM. Here, the Fermi level of the system is set to be zero. As the applied gate voltage increases, both the transmission spectra of two molecules move leftwards, which means that the energy levels shift down with the increasing gate voltage. For AM, when the gate voltage is between  $-2 \text{ V}$  and  $0 \text{ V}$ , the perturbed HOMO (p-HOMO, marked with a downward triangular) of AM is close to the Fermi level of the system, which is the dominant charge transport channel. As the gate voltage sweeps from  $-2 \text{ V}$  to  $0 \text{ V}$ , p-HOMO gradually shifts away from the Fermi level of the system, decreasing the conductance. When the gate voltage continues increasing from  $0 \text{ V}$  to  $1 \text{ V}$ , p-HOMO continues moving away and perturbed LUMO (p-LUMO, marked as an upward triangular) begins to approach the Fermi level of the system. However, both of them are far away from the Fermi level, indicating an off-resonant transport, which is similar to the experiment results that the low-conductance region keeps expanding until  $V_G$  reaches  $1 \text{ V}$ . As the p-LUMO moves closer to

the Fermi level with the increasing gate voltage, the conductance is enhanced. These simulations clearly explain the reason why the conductance decreases as  $V_G$  changes from  $-2 \text{ V}$  to  $0 \text{ V}$ , while the conductance increases with increasing positive  $V_G$  for AM.

For NM, the trend of transmission spectra shift with the increasing gate voltage is similar to AM. One of the differences is that the shift of transmission spectra of NM is relatively slow, indicating that the response to the gate control of AM is better. When the gate voltage increases from  $-2 \text{ V}$  to  $1 \text{ V}$ , the p-HOMO of NM moves away, decreasing the conductance; when the gate voltage keeps increasing, p-HOMO is quite far away from the Fermi level of the system, but p-LUMO is not near the bias window enough due to the large bandgap of NM, which means there is no charge transport channel near the bias window, resulting in a low conductance. Thus, the off-resonant region continues expanding at  $V_G = 2 \text{ V}$ , which is in agreement with the experimental field-effect properties of NM, though without a diamond-shaped characteristic.

## Conclusions

In conclusion, we demonstrate an azulene-based single-molecule FET with two opposite dipole moments, which is

modulated by ionic liquid gating. Compared with NM-based FETs, AM-based FETs exhibit better gate controllability, whose maximum on-off current ratio reaches  $\sim 200$ , which is about five times higher than that for NM. The higher on-off current ratio for AM is a direct consequence of the unique opposite dipole moments of AM that can reduce the conductance in the off-state. Meanwhile, the diamond shape of the low conductance region in the 2D conductance mapping for AM indicates that the molecular orbitals of AM can be more effectively modulated by the gate, and AM-based FET shows ambipolar characteristics. This can be explained by the higher polarizability of AM that enhances the molecular response to the electric field. Additionally, the effective energy level shift of AM with gate voltages and the small bandgap of AM may also result in the diamond-shaped low-conductance region, which is further proved by the theoretical simulation. Thus, introducing two opposite dipole moments to the single molecule and enhancing the polarizability of the molecule can effectively improve the on-off current ratio and the gate modulation. This work provides an effective way to improve the efficiency of gate control and promotes the development of single-molecule FETs. This kind of single-molecule FET is promising for practical applications such as quantum sensors and logic circuits.

## Author contributions

Huanyan Fu: data curation, investigation, visualization, writing-original-draft. Cong Zhao: visualization, writing-original-draft. Jie Cheng: investigation, writing-original-draft. Shuyao Zhou: data curation, investigation, writing-original-draft. Peizhen Peng: investigation. Jie Hao: visualization. Zhirong Liu: supervision, resources. Xike Gao: supervision, resources, conceptualization. Chuancheng Jia: supervision, conceptualization, writing-review & editing, funding acquisition. Xuefeng Guo: supervision, conceptualization, writing-review & editing, funding acquisition.

## Conflicts of interest

There are no conflicts to declare.

## Acknowledgements

We acknowledge primary financial supports from the National Key R&D Program of China (2017YFA0204901, 2021YFA1200101 and 2021YFA1200102), the National Natural Science Foundation of China (22150013, 22173050, 21727806 and 21933001), the Tencent Foundation through the XPLOER PRIZE, "Frontiers Science Center for New Organic Matter" at Nankai University (63181206), the Natural Science Foundation of Beijing (2222009) and Beijing National Laboratory for Molecular Sciences (BNLMS202105).

## References

- 1 A. Aviram and M. A. Ratner, *Chem. Phys. Lett.*, 1974, **29**, 277–283.
- 2 D. Xiang, X. Wang, C. Jia, T. Lee and X. Guo, *Chem. Rev.*, 2016, **116**, 4318–4440.
- 3 N. Xin, J. Guan, M. A. Ratner, C. Zhou, X. Chen, C. Gu, A. Nitzan, J. Fraser Stoddart, Y. Li and X. Guo, *Nat. Rev. Phys.*, 2019, **1**, 211–230.
- 4 H. Chen and J. Fraser Stoddart, *Nat. Rev. Mater.*, 2021, **6**, 804–828.
- 5 A. Bachtold, P. Hadley, T. Nakanishi and C. Dekker, *Science*, 2001, **294**, 1317–1320.
- 6 H. Fu, X. Zhu, P. Li, M. Li, L. Yang, C. Jia and X. Guo, *J. Mater. Chem. C*, 2022, **10**, 2375–2389.
- 7 P. Li, C. Jia and X. Guo, *Chem. Rec.*, 2021, **21**, 1284–1299.
- 8 S. Richter, E. Mentovich and R. Elnathan, *Adv. Mater.*, 2018, **30**, 1706941.
- 9 L. Meng, N. Xin, C. Hu, H. A. Sabea, M. Zhang, H. Jiang, Y. Ji, C. Jia, Z. Yan, Q. Zhang, L. Gu, X. He, P. Selvanathan, L. Norel, S. Rigaut, H. Guo, S. Meng and X. Guo, *Nat. Commun.*, 2022, **13**, 1410.
- 10 P. Wang, C. Jia, Y. Huang and X. Duan, *Matter*, 2021, **4**, 552–581.
- 11 C. Jia, Z. Lin, Y. Huang and X. Duan, *Chem. Rev.*, 2019, **119**, 9074–9135.
- 12 Z. Yan, X. Li, Y. Li, C. Jia, N. Xin, P. Li, L. Meng, M. Zhang, L. Chen, J. Yang, R. Wang and X. Guo, *Sci. Adv.*, 2022, **8**, eabm3541.
- 13 W. Liang, M. P. Shores, M. Bockrath, J. R. Long and H. Park, *Nature*, 2002, **417**, 725–729.
- 14 C. B. Winkelmann, N. Roch, W. Wernsdorfer, V. Bouchiat and F. Balestro, *Nat. Phys.*, 2009, **5**, 876–879.
- 15 M. L. Perrin, C. J. Verzijl, C. A. Martin, A. J. Shaikh, R. Eelkema, J. H. van Esch, J. M. van Ruitenbeek, J. M. Thijssen, H. S. van der Zant and D. Dulic, *Nat. Nanotechnol.*, 2013, **8**, 282–287.
- 16 E. Burzuri, Y. Yamamoto, M. Warnock, X. Zhong, K. Park, A. Cornia and H. S. van der Zant, *Nano Lett.*, 2014, **14**, 3191–3196.
- 17 J. Bai, A. Daaoub, S. Sangtarash, X. Li, Y. Tang, Q. Zou, H. Sadeghi, S. Liu, X. Huang, Z. Tan, J. Liu, Y. Yang, J. Shi, G. Meszaros, W. Chen, C. Lambert and W. Hong, *Nat. Mater.*, 2019, **18**, 364–369.
- 18 X. Xie, P. Li, Y. Xu, L. Zhou, Y. Yan, L. Xie, C. Jia and X. Guo, *ACS Nano*, 2022, **16**, 3476–3505.
- 19 P. Li, C. Jia and X. Guo, *Chin. J. Chem.*, 2021, **39**, 223–231.
- 20 H. Song, Y. Kim, Y. H. Jang, H. Jeong, M. A. Reed and T. Lee, *Nature*, 2009, **462**, 1039–1043.
- 21 W. Y. Kim and K. S. Kim, *Acc. Chem. Res.*, 2010, **43**, 111–120.
- 22 M. L. Perrin, E. Burzuri and H. S. van der Zant, *Chem. Soc. Rev.*, 2015, **44**, 902–919.
- 23 G. D. Scott and T. C. Hu, *Phys. Rev. B*, 2017, **96**, 144416.
- 24 B. Xu, X. Xiao, X. Yang, L. Zang and N. Tao, *J. Am. Chem. Soc.*, 2005, **127**, 2386–2387.
- 25 W. Su, J. Jiang, W. Lu and Y. Luo, *Nano Lett.*, 2006, **6**, 2091–2094.

- 26 N. J. Kay, S. J. Higgins, J. O. Jeppesen, E. Leary, J. Lycoops, J. Ulstrup and R. J. Nichols, *J. Am. Chem. Soc.*, 2012, **134**, 16817–16826.
- 27 C. Jia, M. Famili, M. Carlotti, Y. Liu, P. Wang, I. M. Grace, Z. Feng, Y. Wang, Z. Zhao, M. Ding, X. Xu, C. Wang, S. Lee, Y. Huang, R. C. Chiechi, C. J. Lambert and X. Duan, *Sci. Adv.*, 2018, **4**, eaat8237.
- 28 N. Xin, X. Li, C. Jia, Y. Gong, M. Li, S. Wang, G. Zhang, J. Yang and X. Guo, *Angew. Chem., Int. Ed.*, 2018, **57**, 14026–14031.
- 29 Y. H. Wang, F. Yan, D. F. Li, Y. F. Xi, R. Cao, J. F. Zheng, Y. Shao, S. Jin, J. Z. Chen and X. S. Zhou, *J. Phys. Chem. Lett.*, 2021, **12**, 758–763.
- 30 T. A. Su, M. Neupane, M. L. Steigerwald, L. Venkataraman and C. Nuckolls, *Nat. Rev. Mater.*, 2016, **1**, 16002.
- 31 N. Xin, X. Kong, Y. P. Zhang, C. Jia, L. Liu, Y. Gong, W. Zhang, S. Wang, G. Zhang, H. L. Zhang, H. Guo and X. Guo, *Adv. Electron. Mater.*, 2020, **6**, 1901237.
- 32 F. Schwarz, M. Koch, G. Kastlunger, H. Berke, R. Stadler, K. Venkatesan and E. Lortscher, *Angew. Chem., Int. Ed.*, 2016, **55**, 11781–11786.
- 33 M. Beer and H. C. Longuet-Higgins, *J. Chem. Phys.*, 1955, **23**, 1390–1391.
- 34 R. Pariser, *J. Chem. Phys.*, 1956, **25**, 1112–1116.
- 35 J. Michl and E. W. Thulstrup, *Tetrahedron*, 1976, **32**, 205–209.